HIGH POWER LASER
SCIENCE AND ENGINEERING

RESEARCH ARTICLE

Passive spherical aberration compensation in laser diode side-pumped master oscillator power amplifier laser systems

Pengfei Li[1,2], Yulei Wang[1,2], Fei Zhang[1,2], Yan Li[1,2], Hao Zheng[1,2], Chen Cao[1,2], Kai Li[1,2], Mengyu Jia[1,2], Bingzheng Yan[1,2], Zhenxu Bai[1,2], Yu Yu[1,2], and Zhiwei Lv[1,2]

[1] *Center for Advanced Laser Technology, Hebei University of Technology, Tianjin, China*

[2] *Hebei Key Laboratory of Advanced Laser Technology and Equipment, Tianjin, China*

Abstract

Based on a 4*f* system, a 0° reflector and a single laser diode side-pump amplifier, a new amplifier is designed to compensate the spherical aberration of the amplified laser generated by a single laser diode side-pump amplifier and enhance the power of the amplified laser. Furthermore, the role of the 4*f* system in the passive spherical aberration compensation and its effect on the amplified laser are discussed in detail. The results indicate that the amplification efficiency is enhanced by incorporating a 4*f* system in a double-pass amplifier and placing a 0° reflector only at the focal point of the single-pass amplified laser. This method also effectively uses the heat from the gain medium (neodymium-doped yttrium aluminium garnet) of the amplifier to compensate the spherical aberration of the amplified laser.

Keywords: high beam quality; high conversion efficiency; master oscillator power amplifier; solid-state laser; spherical aberration compensation

1. Introduction

The goal of solid-state laser development is to achieve high beam quality and high-power output[1,2]. This objective is particularly important in fields such as medicine[3-5], LiDAR[6], laser ranging[7] and laser processing[8,9]. The master oscillator power amplifier (MOPA) system, recognized for its capability of staged amplification and precise control of beam quality, offers significant advantages in the pursuit of high-power lasers. However, during the amplification process, thermal accumulation effects can cause a deterioration in beam quality, which significantly limits the applications of these lasers. Therefore, it is essential to improve the beam quality of high-power solid-state lasers as part of ongoing development efforts.

In recent years, researchers have generally explored two main approaches. The first approach is to enhance the beam quality of lasers by mitigating the thermal effects of the gain medium[10,11]. Various methods alleviate thermal effects in crystals. One approach is to increase the heat exchange area between the crystal and the cooling system, which improves heat dissipation[12,13]. Another method involves using temperature control systems to regulate the temperature around the crystal[14,15]. In addition, adjusting the distribution of the pump and seed laser improves the beam quality of the amplified laser[16,17]. However, under high-power pumping, gain crystals still encounter adverse effects, such as thermal lensing, thermal depolarization and thermally induced birefringence. These phenomena can transform gain crystals from planar surfaces into lenses with significant spherical aberration (SA), leading to a decrease in beam quality and pump laser utilization efficiency. The second approach involves introducing specialized optical devices into the optical path to compensate for the SA of the laser[18]. Spherical aberration compensators (SACs) are commonly used to correct the wavefront of the amplified laser[19–21], thereby improving the beam quality of the amplified laser. However, the SA within a MOPA system varies with increasing pump power, while the externally introduced SA remains constant. This variability necessitates a series of SACs with different parameters for compensation,

Correspondence to: Y. Wang, Center for Advanced Laser Technology, Hebei University of Technology, Tianjin 300401, China. Email: wyl@hebut.edu.cn

1
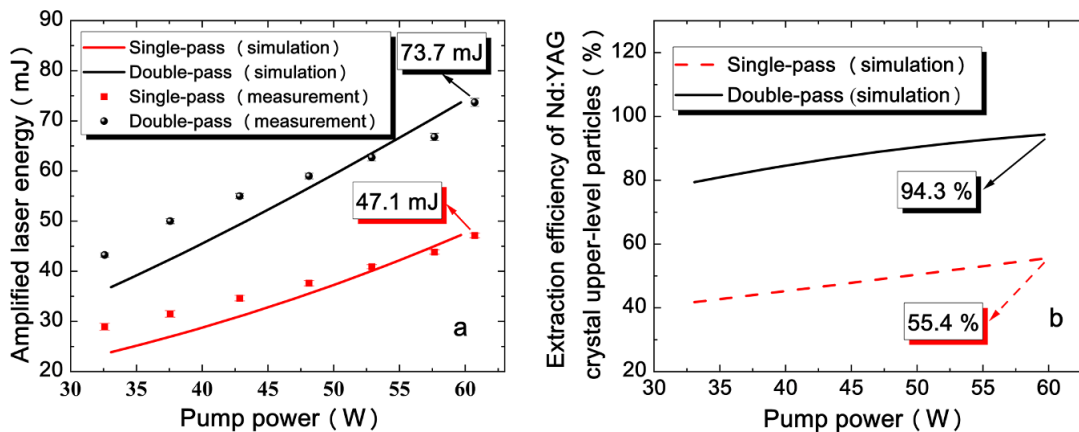
Figure 1. Under varying pump powers: (a) the variation in single-pass and double-pass amplified laser energy; (b) the variation in the upper-state particle extraction efficiency of the Nd:YAG crystal for both single-pass and double-pass amplifications.

adding complexity to the laser system[22]. Although these studies significantly improve the beam quality of the amplified laser, research on compensating for SA introduced by thermal lens effects using the gain medium's own heat is relatively limited. Therefore, it is necessary to further study this issue.

To address the deterioration of the beam quality in MOPA lasers based on neodymium-doped yttrium aluminium garnet (Nd:YAG) crystal rod, this paper proposes a scheme to passively compensate for the SA introduced by the thermal effects of the crystal rod, and simultaneously enhance the amplification capability of the laser diode (LD) side-pumped amplifier. Firstly, we discuss the optimization effect of the 4*f* system on the amplified laser in the passive SA compensation and then compare the beam qualities M^2 (M_y^2, M_x^2) of the amplified lasers in the MOPA system for the seed laser after single-pass and double-pass amplification through the LD side-pumped amplifier. In double-pass amplification, we mainly consider three scenarios involving 0° mirrors: positioned at the focal point of the single-pass amplified laser; 1 m in front of the focal point; and 1 m behind the focal point. When the 0° reflector is placed at the focal point of the amplified laser in the LD single-pass amplified laser, and the 4*f* system is incorporated into the double-pass amplifier, the SA introduced by the thermal effects in the Nd:YAG crystal and the imprecise adjustment of the 4*f* system is effectively compensated. This laser configuration also fully extracts the upper-state particles from the Nd:YAG crystal rod and optimizes the optical field shape of the amplified laser. Therefore, when the pump power is 60.7 W, the improved laser configuration obtains the amplified laser with a repetition rate of 300 Hz, a single-pulse energy of 73.7 mJ, a pulse width of 30 ns, a root-mean-square (RMS) of 1.17% (30 min), $M_y^2 = 1.22$ and $M_x^2 = 1.37$.

2. Theoretical model

In the amplifier experiment employing double-pass amplification, the effective length of the Nd:YAG crystal is 15.6 cm. Figure 1 simulates the output energy and the upper-state particle extraction efficiency of the Nd:YAG crystal under different pumping powers, based on the parameters from Refs. [23,24], for both double-pass and single-pass amplifications. As shown in Figure 1, at a pump power of 60.7 W, double-pass amplification increases the single-pulse energy of the amplified laser from 47.1 to 73.7 mJ compared to single-pass amplification, while also improving the upper-state particle extraction efficiency of the Nd:YAG crystal from 55.4% to 94.3%. This result is consistent with subsequent experimental measurements, indicating that double-pass amplification can effectively enhance the optical-to-optical conversion efficiency of the LD side-pumped amplifier while simultaneously enhancing the amplification capability of the LD side-pumped amplifier. However, due to heat accumulation within the gain medium, the beam quality and optical field shape of the amplified laser deteriorate sharply. Therefore, it is an urgent problem to improve the beam quality and optical field shape of the double-pass amplified laser.

During the amplification process, a temperature gradient develops within the gain medium, causing the refractive index of the rod-shaped gain medium to change with temperature according to a second-order approximation. This change results in a radial gradient distribution of the crystal's thermal-optical coefficient dn/dT, leading to variations in thermal conduction performance at different positions. Consequently, the optical power $D(r)$ becomes a function of the radial coordinate r, and the planar crystal is transformed into a lens exhibiting SA. The relationship between the pump power and the thermal lens focal length of the Nd:YAG
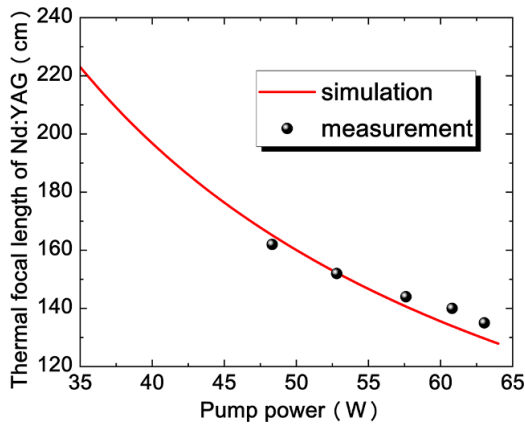
Figure 2. Variation of the thermal focal length of the Nd:YAG crystal rod at different pump power levels.
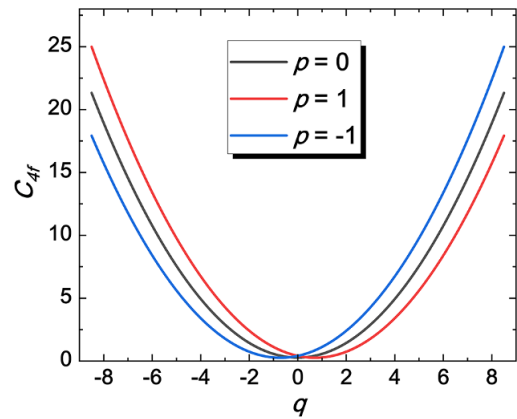

Figure 3. Relationship graph between the dimensionless aberration coefficient C_{4f} for a lens as a function of the lens-shape factor q and the imaging parameter p.

crystal rod[25,26] is as follows:

$$f_{\mathrm{T}} = \frac{k\pi R^2}{\eta P_{\mathrm{in}}} \left[\frac{1}{2} \frac{\mathrm{d}n}{\mathrm{d}T} + n_0{}^3 \alpha C_{\mathrm{r}.\phi} + \frac{\alpha R(n_0-1)}{L} \right]^{-1}. \quad (1)$$

In the equation, R represents the rod radius, α is the coefficient of thermal expansion, $\frac{\mathrm{d}n}{\mathrm{d}T}$ is the refractive index temperature coefficient, n_0 is the refractive index of the crystal rod before being pumped and $C_{\mathrm{r}.\phi}$ is the photoelastic coefficient of the Nd:YAG crystal rod. At different pump laser powers, the relationship between the thermal focal length of the crystal rod and the pump laser power, based on Equation (1), is shown by the red line in Figure 2. The five black points in Figure 2 correspond to the measured thermal focal lengths of the amplified laser for pump powers of 48.3, 52.8, 57.6, 60.7 and 63.04 W, which are 162, 152, 144, 140 and 135 cm, respectively. As shown in Figure 2, the simulated thermal focal lengths closely match the measured data. This indicates that as the pump power increases, the thermal focal length of the Nd:YAG crystal gradually decreases. This leads to significant thermal effects within the Nd:YAG crystal, resulting in a decrease in amplified laser output power and deterioration in beam quality. Therefore, optimizing the SA introduced by thermal effects in the optical path is crucial for improving laser beam quality.

If the optical path contains optical elements with SA, the beam quality factor M^2 of the output laser is determined by both the initial beam quality factor $M_{\mathrm{r}0}{}^2$ and an additional factor $M_{\mathrm{rq}}{}^2$ attributable to SA[27,28]. Therefore, under constant seed laser conditions, the final M^2 of the amplified laser output is ultimately determined by $M_{\mathrm{rq}}{}^2$, where $M_{\mathrm{rq}}{}^2$ is as follows:

$$M_{\mathrm{rq}}{}^2 = \frac{8\pi \beta_{\mathrm{r}}}{\lambda} C_4 r^4. \quad (2)$$

Here, C_4 is the coefficient of the fourth-order aberration caused by SA. As indicated by Equation (2), the magnitude

of C_4 directly affects the $M_{\mathrm{rq}}{}^2$ of the laser. During the MOPA amplification process, thermal effects in the gain medium cause the Nd:YAG crystal rod to function effectively as a lens, at which point C_4[29] is as follows:

$$C_4 = \pm \frac{C_{4\mathrm{f}}}{f^3}, \quad (3)$$

where the dimensionless aberration coefficient $C_{4\mathrm{f}}$ is as follows:

$$C_{4\mathrm{f}} = \frac{n^3 + (3n+2)(n-1)^2 p^2 + (n+2) q^2 + 4(n^2-1) pq}{32n(n-1)^2}. \quad (4)$$

In the refractive index of the medium n and laser imaging parameter p, positive and negative values represent positions in front of and behind the laser focal point, respectively. Figure 3 simulates the relationship between p when it is 0, -1, and $+1$, and $C_{4\mathrm{f}}$ with the lens shape factor q (where $q = 0$ corresponds to a symmetric lens, and the cases $q = \pm 1$ correspond to plano-curved or curved-plano lenses). As shown in Figure 3, when the amplifier uses double-pass amplification, if a 0° mirror is placed at the focal point of the single-pass amplified beam, the heat generated by the LD side-pumped amplifier is the same, the laser imaging parameters p are opposite and the lens shape factor q is either identical or opposite, resulting in identical $C_{4\mathrm{f}}$ values at the same distance on either side of the laser focal point. This condition causes the fourth-order aberration coefficient C_4 to be opposite at equal distances from the laser focal point. During amplification, due to the thermal lens effect of the crystal, placing a 0° mirror at the focal point of the single-pass beam will result in the $M_{\mathrm{rq}}{}^2$ factor, which causes deterioration in beam quality due to SA, being cancelled out when the beam passes through the Nd:YAG crystal twice. Theoretically, this method can mitigate the degradation of
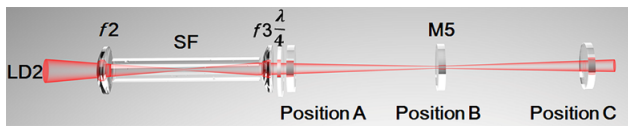
Figure 4. The diagram showing the variation in the optical field diameter of the single-pass amplified laser output from amplifier.

the amplified beam's M^2 caused by thermal lensing, thereby improving the beam quality of the amplified laser.

Based on the aforementioned theory, this paper proposes a novel double-pass amplification device using Nd:YAG crystals. The device consists of a side-pumped amplifier LD2, a 4f system (including lenses f2, f3 and SF), a quarter-wave plate and a 0° reflector mirror, M5. Figure 4 shows the change in the beam diameter of the single-pass amplification laser field. When the laser passes through the single-pass amplification of the LD2 side-pumped amplifier[30], the thermal lensing effect of the Nd:YAG crystal causes the beam to focal point initially, followed by divergence beyond the focal point. This phenomenon is consistent with the theory of SA before and after the focal point is opposite[31,32]. If the 0° reflector mirror M5 is precisely placed at the focal point B for double-pass amplification, it utilizes the SA caused by the thermal lens effect in the Nd:YAG crystal for mutual compensation. This not only improves beam quality and prevents degradation, but also enhances the extraction of upper-state particles in the Nd:YAG crystal, significantly boosting the amplifier's efficiency. In addition, the 4f system integrated into the amplification setup increases the misalignment sensitivity of the laser system, decreases the spatial frequency spectrum of the beam, corrects the beam's spot uniformity and maintains beam coherence. It also optimizes the mode structure of the amplified beam and compensates for beam distortions. These features effectively improve beam quality and optimize optical field distortion, leading to high-quality laser output. Through this optical design, the double-pass amplification system enhances the optical-to-optical conversion efficiency and achieves laser pulse output with high beam quality and near-Gaussian laser fields.

3. Experimental setup

Figure 5 shows a MOPA laser system, notable for its high beam quality and efficiency. The seed laser is obtained through an electro-optic Q-switching oscillator. The resonator comprises a stable plane–plane cavity formed by mirrors M1 and M2. Mirror M1 is a 0° high-reflection (HR) mirror at a wavelength of 1064 nm, while mirror M2 is a partially transmitting mirror with a transmission rate of 50% at 1064 nm. The cavity length measures 780 mm. LD1 is a 1200 W side-pump amplifier, which utilizes a 0.6% doped $\phi 3 \times 78$ mm Nd:YAG crystal as the gain medium, and an

anti-reflection (AR) film at 1064 nm is coated on the crystal surface. The system produces laser pulses with a repetition rate of 300 Hz, a single-pulse energy of 9.46 mJ, an RMS of 1.6% (over 30 min), beam quality factors of $M_y^2 = 1.21$ and $M_x^2 = 1.30$, a pulse width of 30 ns and a central wavelength of 1064.7 nm. This setup provides a high-quality seed laser for subsequent amplification.

To avoid issues such as beam distortion and gain loss caused by low efficiency in the overlapping beams of the amplifier, we use a 2000 W LD2 side-pump module as the amplifier in the MOPA system. The gain medium is a $\phi 4 \times 78$ mm Nd:YAG crystal rod with a doping concentration of 0.6% (AR at 1064 nm). An isolation device with a centre wavelength of 1064 nm is positioned after the oscillator. This device, composed of PBS2, a Faraday rotator (FR), a half-wave plate and PBS3, reduces the likelihood of self-oscillation during amplification and protects the optical components in the oscillator from residual depolarized radiation.

Since the output laser from the oscillator is a focused beam, a concave lens (f1) with a focal length of 786 mm (AR at 1064 nm) is used in the experiment to match the oscillator's output laser with the crystal in the LD2 side-pump amplifier. This setup increases the overlap area between the seed laser and the gain medium, thereby enhancing the amplification efficiency of the amplifier. After the seed laser from the oscillator is introduced into the LD2 side-pump amplifier for single-pass amplification, a 4f system is placed after the LD2 side-pumped amplifier to enhance the stability of the amplification system and its misalignment sensitivity.

The beam passes through the 4f imaging system (AR at 1064 nm) and then through a quarter-wave plate (AR at 1064 nm). After being reflected by a 0°high-reflection mirror M5 (HR at 1064 nm) located at the focal point B of the single-pass laser, the laser beam returns along the same path. It subsequently passes through the quarter-wave plate again, converting circular polarization to S-polarization, before re-entering the LD2 side-pump amplifier for secondary amplification. Under the conditions of a cooling water temperature of 21°C, a flow rate of 14.7 L/min and a pump power of 60.7 W, the MOPA system outputs laser pulses through PBS4, achieving a repetition rate of 300 Hz, a single-pulse energy of 73.7 mJ, a pulse width of 30 ns and an RMS (30 min) of 1.17%. The beam quality factors are $M_y^2 = 1.22$ and $M_x^2 = 1.37$.

The temporal characteristics of the laser beam are measured by combining a rapid photodetector (UPD-35-UVIR-D, Alphalas GmbH, Germany; rise time < 35 ps) with a digital oscilloscope (DPO71254C, Tektronix, USA; bandwidth 12.5 GHz; sampling rate 100 Gsamples/s). The laser pulse energy is measured by an energy meter (Vega Pyroelectric PE50DIF-ER (s/n:917609), Ophir Optronics, Israel). The beam quality factors M_y^2, M_x^2 of the laser are measured by an M^2 instrument (M2Beam U3 VIS-NIR, Duma Optronics Ltd., Israel).
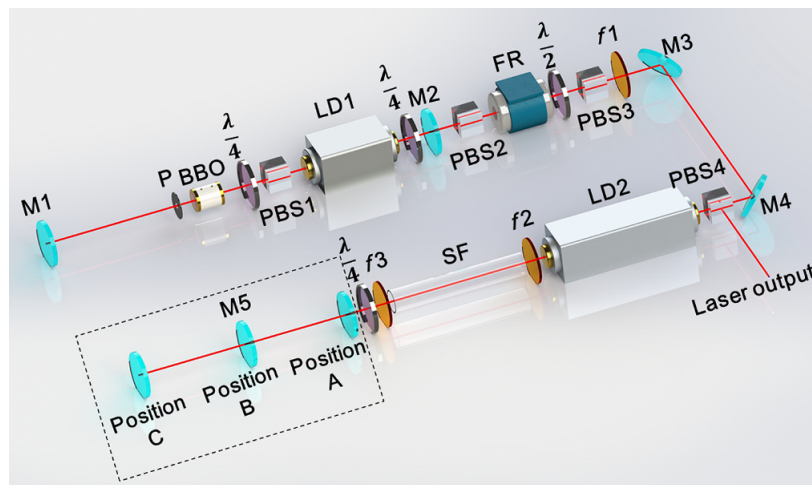
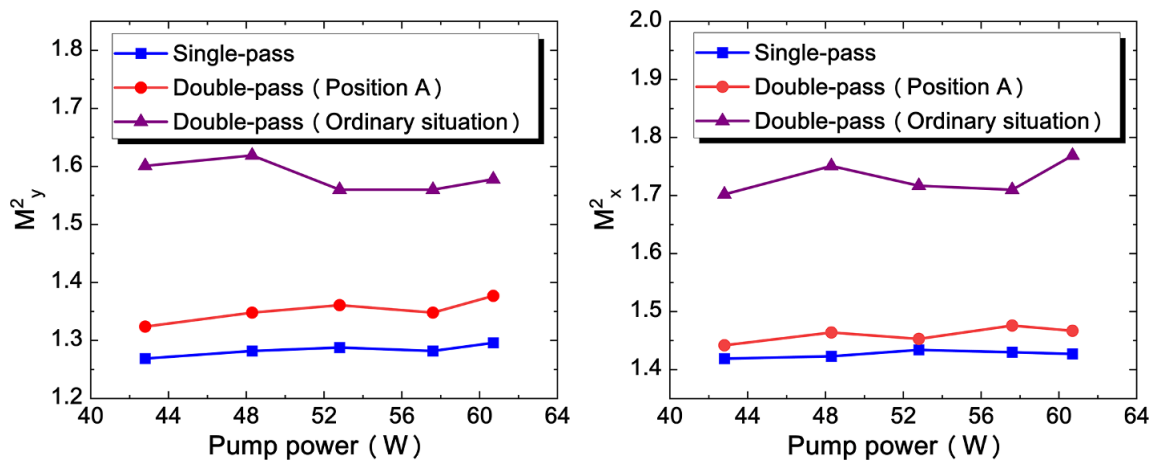**Figure 5.** High beam quality, high-efficiency MOPA laser system.

Figure 6. At varying pump power levels, the laser beam quality factors M_y^2, M_x^2 are assessed for single-pass amplification through the side-pump amplifier LD2, double-pass amplification with M5 positioned at location A and ordinary double-pass amplification without the $4f$ system.

4. Results and discussion

4.1. Effects of the novel bidirectional amplification 4f system on amplified laser energy and beam quality

To analyse the effects of the $4f$ system on the amplified laser energy and the beam quality in novel bidirectional amplification, we discuss the values of M^2 in three cases: the laser undergoes single-pass amplification through the side-pump amplifier LD2; double-pass amplification with M5 placed at position A (Figure 5); and ordinary double-pass amplification without the $4f$ system (i.e., double-pass amplification that places a quarter-wave plate and a 0° mirror next to each other behind the side-pump amplifier LD2 in turn). The results are shown in Figure 6. Subsequently, we analyse the relationship between pump power and amplified laser energy for double-pass amplification with M5 placed at position A (Figure 5) and ordinary double-pass amplification without the $4f$ system. The results are shown in Figure 7.

As can be seen from Figures 6 and 7, when the pump power is set to 60.7 W and the $4f$ system is incorporated into the double-pass amplification system, compared with the ordinary double-pass amplification system, the single-pulse energy of the amplified laser is nearly unchanged, and the beam qualities along the y-axis and x-axis improve by 0.2 and 0.3, respectively. Therefore, the $4f$ system improves the misalignment sensitivity of the laser system, reduces beam nonuniformity and corrects astigmatism, thereby improving the beam quality of the amplified laser.

4.2. Effects of the novel bidirectional amplification on the beam quality, the optical field distribution and the energy of amplified laser

Considering that the SA introduced by the thermal effect of the Nd:YAG crystal in LD2 side-pump amplifier is not compensated, the beam quality of the double-pass
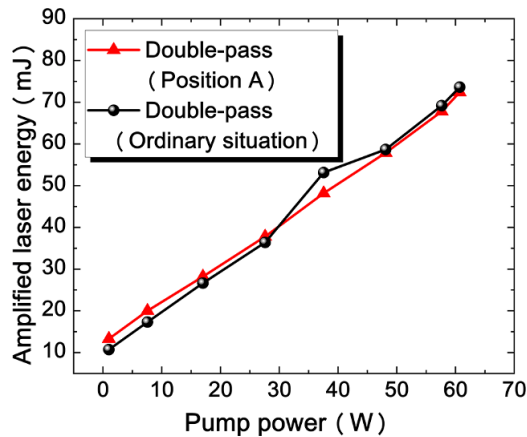
Figure 7. The single-pulse energy of the double-pass amplified laser, with mirror M5 positioned at location A under varying pump powers, is compared to the single-pulse energy of the ordinary double-pass amplified laser without the 4*f* system.

amplification with M5 placed at position A is still lower than that of the single-pass amplification. A solution is given in Section 2. Let us verify the feasibility of this scheme. Firstly, adjust the position of M5 using a manual translation stage for different pump power levels, ensuring it is precisely positioned at the focal point of the output beam after the laser undergoes single-pass amplification through the side-pumped LD2. Secondly, the M2Beam U3 is employed to measure the M^2 values of the amplified laser at different pump power during single-pass amplification with the side-pumped amplifier LD2. As well as the values of M^2 at different pumping powers during double-pass amplification with the side-pumped amplifier LD2 when the 0° mirror M5 is placed at position B, the values are also measured at points A and C, respectively, where B represents the focal point of the single-pass amplified laser in Figure 5, A is 1 m in front of focal point B and C is 1 m behind focal point B. Figure 8 shows the values M_y^2, M_x^2 of the amplified laser

for the various pump powers. As illustrated in Figure 8, the beam quality of the double-pass amplification with M5 positioned at either A or C is inferior to that of single-pass amplification for the various pump powers. This is because during the amplification process, when the amplified laser passes through the Nd:YAG crystal and the f2 and f3 lenses in the 4*f* system twice before and after, the absolute values of the laser parameter *p* are different. Therefore, the SAs introduced by the thermal lens of the crystal and the positional errors of f2 and f3 in the 4*f* system when the laser passes through side-pumped amplifier LD2 for the first time does not cancel each other out with the SA when it passes through side-pumped amplifier LD2 for the second time. This results in an increased M_{rq}^2 of the amplified beam and a deterioration in beam quality. If M5 is placed at focal point B, the SA introduced by the thermal effect of Nd:YAG crystals in the second amplification process can almost offset the SA introduced in the first, so the beam quality of the double-pass amplified laser is higher than that of the single-pass amplified laser. Similarly, the SA caused by the position errors of f2 and f3 in the 4*f* system can also be compensated. Therefore, when the laser passes through the side-pumped amplifier LD2 for double-pass amplification, effective compensation for the degradation of beam quality caused by the thermal lensing effect in the Nd:YAG crystal occurs only when the 0° mirror M5 is positioned at focal point B of the single-pass amplified laser.
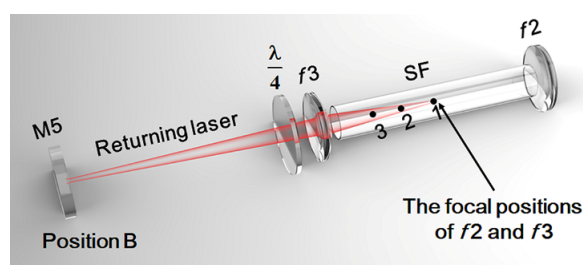
Next, we discuss the optical field shape of the amplified laser when M5 is placed at positions A, B and C. Figure 9 shows the optical field shape of the double-pass amplified laser at the distances of 25 and 120 cm from the laser output port when the pump power is 60.7 W. From Figure 9, no matter where M5 is placed, whether at A, B or C, the optical field shape of the amplified laser at the distance of 120 cm from the laser output port has no obvious distortion. However, when M5 is at positions A and C, the optical field shape of the amplified laser from 25 cm of the laser output
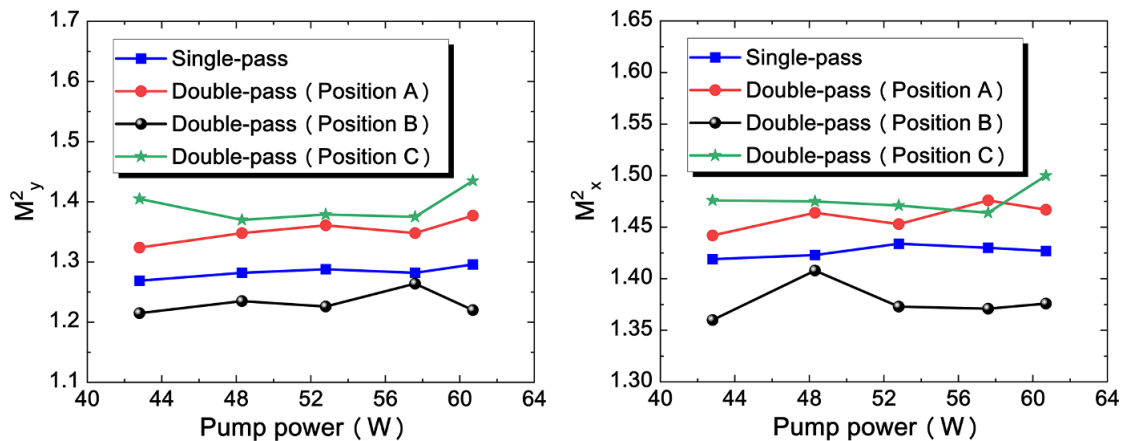
Figure 8. At varying pump power levels, the beam quality factors M_y^2, M_x^2 for the LD2 amplified laser in single-pass configuration and M_y^2, M_x^2 for the amplified laser with M5 placed in positions A, B and C in double-pass configuration.

| The optical field shape of the amplified laser at a distance of 25 cm from the laser output port. | Position A | Position B | Position C |
| The optical field shape of the amplified laser at a distance of 120 cm from the laser output port. | Position A | Position B | Position C |
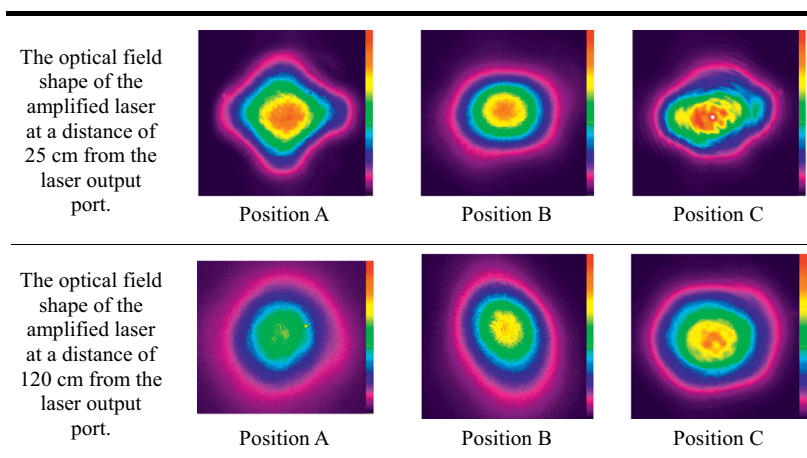
Figure 9. Under a pump power of 60.7 W, when the mirror M5 is positioned at locations A, B and C, the laser undergoes double-pass amplification through the side-pumped amplifier LD2. The distribution of the optical field shape is measured at distances of 25 and 120 cm from the output aperture.

Figure 10. When M5 is positioned at A, B and C, the amplified laser reflected by M5 reaches the focal points at SF (positions 3, 1 and 2, respectively).

port is seriously distorted. When M5 is positioned at B, the optical field shape of the amplified laser at 25 cm away from the laser output port approximately follows the Gaussian distribution. This is because if M5 is at position A or C, the focal point of the returned laser is position 3 or position 2 of SF in Figure 10, which deviates from the common focal point 1 of lenses f2 and f3 in the 4f system. Thus, the laser is not focused well enough, and the optical field shape of the output laser is deformed to different degrees. When M5 is placed at position B, then the focal point of the returned laser is position 1 in Figure 10. Therefore, the 4f system can effectively perform space filtering, and the double-pass amplification achieves the optimal optical imaging and wavefront modulation, and obtains the amplified laser approximately following the Gaussian distribution.

The new double-pass amplifier not only significantly improves the beam quality and optical field shape of the amplified laser, but also enhances the amplification efficiency of the side-pumped amplifier LD2. As shown in Figure 11, when the pump power is 60.7 W, compared with the single-pass amplification, the energy of the output laser increases from 47.1 to 73.7 mJ in the new double-pass amplification when M5 is placed at position B in Figure 5.

In addition, the optical-to-optical conversion efficiency improves from 18.1% to 31.4%. Furthermore, the ratio of the depolarization of the amplified laser to its total energy is reduced from 7.4% to 1.2%. This is because the heat value of the Nd:YAG crystal obtained by the laser twice through the side-pumped amplifier LD2 is almost equal. The phase difference introduced by the laser passing through the crystal second time can offset the phase difference in the first, and the depolarization caused by the thermal stress birefringence of the crystal decreases.

5. Conclusion

This paper uses the thermal energy of Nd:YAG crystal to compensate the SA caused by the thermal lens effect, so as to effectively improve the beam quality of the amplified laser output from MOPA laser systems. By adding a 4f system after the side-pumped amplifier LD2, we improve the misalignment sensitivity of the laser system and realize the dual spatial filtering and wavefront modulation, so as to improve the beam quality and optical field shape of the amplified laser. When the laser undergoes double-pass amplification through the side-pumped amplifier LD2 and the 0° mirror is at focal point B of the single-pass amplification, the SA introduced by the thermal lens of the Nd:YAG crystal, the position errors of f2 and f3 in the second amplification offsets the SA introduced in the first amplification. Thus, this prevents the degradation of beam quality caused by the thermal effects of the crystal, and ensures that the beam quality of the double-pass amplification is better than that of the single-pass amplification. Compared with the single-pass amplification, the new double-pass amplification not only uses the heat of the Nd:YAG crystal to compensate the thermal depolarization caused by the thermal effects of the crystal, but also improves the extraction efficiency of
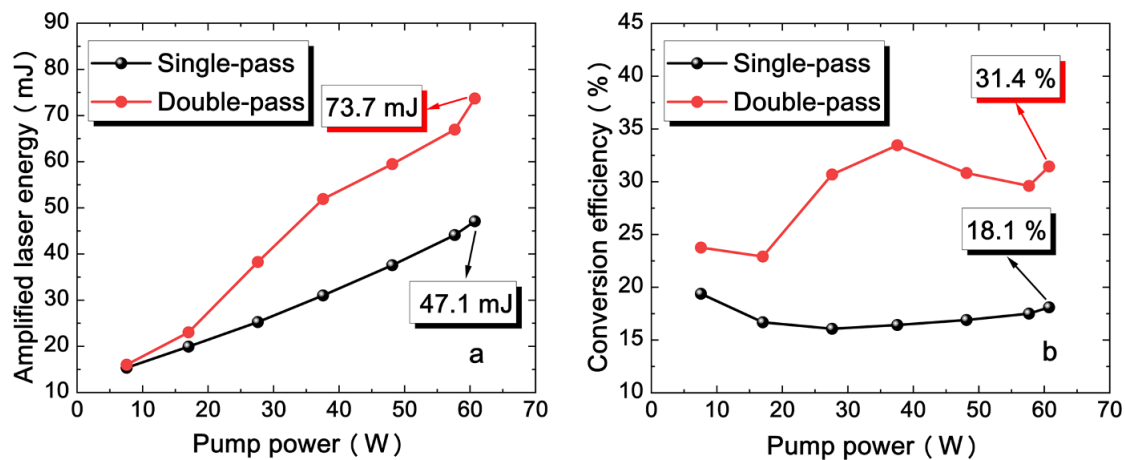
Figure 11. When the laser undergoes single-pass and double-pass amplification through the side-pumped amplifier LD2: (a) the relationship between the pump power and amplified laser energy; (b) the relationship between the pump power and optical-to-optical conversion efficiency.

the upper-state particles in the gain medium. Therefore, this scheme is also applicable to the amplifiers at various stages in the MOPA laser system under the condition of ensuring the safety of the optical components. This provides support for optimizing the amplification capability, beam quality and optical field shape of the MOPA laser system.

Acknowledgements

References

1. S. Nagel, B. Metzger, D. Bauer, J. Dominik, T. Gottwald, V. Kuhn, A. Killi, T. Dekorsy, and S. Schad, Opt. Lett. **46**, 965 (2021).
2. M. Zeyen, L. Affolter, M. A. Ahmed, T. Graf, O. Kara, K. Kirch, M. Marszalek, F. Nez, A. Ouf, R. Pohl, I. Schulthess, S. Rajamohanan, P. Yzombard, K. Schuhmann, and A. Antognini, Opt. Express **32**, 1218 (2024).
3. A. Lima, L. Sergio, L. Trajano, B. Souza, J. Mendes, A. Cardoso, C. Figueira, B. Tavares, D. Figueira, A. Mencalha, E. Trajano, and A. Fonseca, Lasers Med. Sci. **35**, 661 (2020).
4. M. Saeed, M. Z. Iqbal, W. Z. Ren, Y. Z. Xia, W. S. Khan, and A. Wu, J. Mater. Chem. B **7**, 210 (2019).
5. Q. Cheng, Y. L. Tian, H. P. Dang, C. C. Teng, K. Xie, D. L. Yin, and L. F. Yan, Adv. Healthcare Mater. **11**, e2101697 (2022).
6. Q. Y. Chen, S. Mao, Z. P. Yin, Y. Yi, X. Li, A. Z. Wang, and X. Wang, Opt. Express **31**, 23931 (2023).
7. Z. N. Wang, L. J. Xu, D. Li, Z. X. Zhang, and X. L. Li, IEEE Sensors J. **21**, 10879 (2021).
8. A. Pento, A. Bukharina, S. Nikiforov, Y. Simanovsky, B. Sartakov, R. Ablizen, V. Fabelinsky, V. Smirnov, and A. Grechnikov, Int. J. Mass Spectrom. **461**, 116498 (2021).
9. B. Henriques, D. Fabris, B. Voisiat, A. Boccaccini, and A. Lasagni, Adv. Funct. Mater. **34**, 2307894 (2023).
10. J. Kasinski and R. Burnham, Appl. Opt. **35**, 5949 (1996).
11. H. Z. Qiao, K. Zhong, F. J. Li, X. Z. Zhang, Y. Z. Zheng, S. J. Wang, T. Gegen, X. Q. Li, D. G. Xu, and J. Q. Yao, Opt. Laser Technol. **164**, 109486 (2023).
12. K. Li, Y. L. Wang, Y. Yu, J. F. Yue, C. Y. Song, C. Cao, Z. K. Li, W. Y. Wang, Z. B. Meng, Z. X. Bai, Y. F. Li, P. D. Zhao, Y. Zhang, and Z. W. Lu, Opt. Laser Technol. **157**, 108717 (2023).
13. W. Zhu, H. J. He, J. Yu, Q. D. Lin, X. Y. Guo, C. T. Zhou, and S. C. Ruan, Opt. Commun. **499**, 127268 (2021).
14. C. Ma, Z. Liu, K. Liu, Y. Yang, X. J. Wang, Y. Bo, D. F. Cui, and Q. J. Peng, Opt. Laser Technol. **148**, 107767 (2022).
15. Q. L. Long, Q. G. Wang, Y. F. Mao, J. P. Gu, L. Wang, and Y. He, Int. J. Therm. Sci. **194**, 108547 (2023).
16. Y. F. Li, B. Zhang, W. L. Cao, W. Chen, D. W. Zhang, K. Ueda, and J. L. Li, Opt. Express **31**, 43657 (2023).
17. J. Y. Li, P. J. Shang, Y. F. Gong, Q. Guo, F. Q. Ma, B. B. Li, L. Q. Li, and S. Y. Wang, Opt. Express **31**, 36859 (2023).
18. J. Meng, C. Li, Z. H. Cong, Z. G. Zhao, S. Wang, G. Y. Liu, and Z. J. Liu, Chin. Opt. Lett. **21**, 051401 (2023).
19. C. Liu, T. Riesbeck, X. Wang, J. H. Ge, Z. Xiang, J. Chen, and H. J. Eichler, Opt. Commun. **281**, 5222 (2008).
20. M. Bonnefois, M. Gilbert, P. Y. Thro, D. Farcage, and J. M. Weulersse, Proc. SPIE **5707**, 362 (2005).
21. Y. Lumer, I. Moshe, S. Jackel, and A. Meir, J. Opt. Soc. Am. B. **27**, 1337 (2010).
22. Q. W. Jin, Y. Pang, J. F. Jiang, L. Tan, L. L. Cui, B. Wei, Y. H. Sun, and C. Tang, Proc. SPIE **10710**, 107103B (2018).
23. W. Koechner, *Solid State Laser Engineering* (Springer, Berlin, 2020), p. 161.
24. C. Y. Li, C. Q. Lu, C. Li, N. Yang, Y. Li, Z. Yang, S. Han, J. F. Shi, and Z. W. Zhou, Opt. Commun. **394**, 1 (2017).
25. Q. F. Ou, G. Y. Feng, D. P. Liu, and C. Z. Li, Laser Technol. **1**, 15 (2017).
26. F. Song, C. B. Zhang, X. Ding, J. J. Xu, and G. Y. Zhang, Appl. Phys. Lett. **81**, 2145 (2002).
27. V. N. Mahajan, J. Opt. Soc. Am. A **3**, P2 (1986).
28. B. J. Neubert and B. Eppich, Opt. Commun. **250**, 241 (2005).
29. A.E. Siegman, Appl. Opt. **32**, 5893 (1993).
30. J. Zhang, Z. Bai, H. Zheng, C. Zhao, Y. Ding, Z. Lu, and Y. Wang, Opt. Express **32**, 39293 (2024).
31. Y. X. Qi, Z. G. Zhao, C. Liu, and Z. Xiang, IEEE J. Sel. Topics Quantum Electron. **21**, 220 (2015).
32. Y. X. Qi, "Side-pumped solid-state laser master oscillator power amplifier with high output power and excellent beam quality," PhD thesis (Zhejiang University, 2024), pp. 23–31.